Earthline Journal of Chemical Sciences
E-ISSN: 2581-9003; CODEN: EJCSB4
Volume 13, Number 3, August 2026, Pages 313-325
https://doi.org/10.34198/ejcs.13326.22.313325

Interaction of captopril with cations of Mg and Ca – A DFT treatment

Lemi Türker

Department of Chemistry, Middle East Technical University, Üniversiteler, Eskişehir Yolu No: 1, 06800 Çankaya/Ankara, Turkey
e-mail: lturker@gmail.com; lturker@metu.edu.tr

Abstract

Captopril is an antihypertensive medicine whose hypotensive activity may result from an inhibitory action on renin-angiotensin system. Presently, captopril and its composites consisting of dications of magnesium and calcium have been investigated thoroughly within the constraints of density functional theory at the level of B3LYP/6-311++G(d,p). The cations considered are important functions in human metabolism. Therefore, their interactions with captopril, at the molecular level have been thought that might enlighten some chemical facts. The collected data have revealed that the optimized structures of them have exothermic heats of formation and favorable Gibbs free energy of formation values. They are thermally favored and electronically stable at the standard states. Various structural and quantum chemical data have been collected and discussed, including IR and UV-VIS spectra.

1. Introduction

Captopril is the first orally active inhibitor of angiotensin-converting enzyme to become available [1,2]. Captopril inhibits the converting enzyme peptidyl dipeptidase that hydrolyzes angiotensin I to angiotensin II and inactivates bradykinin, a potent vasodilator. The hypotensive activity of captopril may result from an inhibitory action on renin-angiotensin system and a stimulating action on the kallikrein-kinin system [2]. In severe hypertension captopril plus a diuretic (and in some patients a βr-blocker) usually reduced blood pressure significantly more than it could be achieved with 'standard triple therapy' [1]. Indeed, at the present stage of the drug's development, patients not responding to or not tolerating 'traditional' antihypertensive therapy represent the most suitable candidates for captopril treatment. Captopril, an angiotensin-converting enzyme (ACE) inhibitor, has been widely used for therapy of arterial hypertension and cardiovascular diseases. However, the protective effects of captopril on hypertension-induced organ damage remain elusive. In spite of the fact that captopril has been well tolerated in most patients, some troublesome or potentially serious side effects have been reported, (including agranulocytosis, dysgeusia and reduced renal function) although a clear causal relationship with captopril was not always established, it would appear that the final place of captopril in the treatment of hypertension may ultimately depend on further clarification of its adverse effects profile [1-3]. Captopril has produced encouraging improvement in a small number of patients with severe congestive heart failure resistant to conventional therapy [1].

In the past captopril, had been the focus of many researchers as its beneficial and detrimental side effects [1,3-12]. For many years, various aspects of captopril have attracted the attention of scientist however in the present study some other interesting features of it at the molecular level in the realm of density functional theory are presented.

Received: June 4, 2026; Accepted: July 8, 2026; Published online: July 16, 2026

Keywords and phrases: captopril, magnesium cation, calcium cation, hypotensive agent, density functional calculations.

2. Method of Calculations

In the present study, all the initial optimizations of the structures leading to energy minima have been achieved first by using MM2 method which is then followed by semi empirical PM3 self consistent fields molecular orbital method [13-15]. Afterwards, the structure optimizations have been achieved within the framework of Hartree-Fock and finally by using density functional theory (DFT) at the level of B3LYP/6-311++G(d,p) [16,17]. Note that the exchange term of B3LYP consists of hybrid Hartree-Fock and local spin density (LSD) exchange functions with Becke's gradient correlation to LSD exchange [18]. The correlation term of B3LYP consists of the Vosko, Wilk, Nusair (VWN3) local correlation functional [19] and Lee, Yang, Parr (LYP) correlation correction functional [20]. In the present study, the normal mode analysis for each structure yielded no imaginary frequencies for the $3N–6$ vibrational degrees of freedom, where N is the number of atoms in the system. This search has indicated that the structure of each molecule considered corresponds to at least a local minimum on the potential energy surface. Furthermore, all the bond lengths have been thoroughly searched in order to find out whether any bond cleavages occurred or not during the geometry optimization process. All these computations were performed by using SPARTAN 06 program [21].

3. Results and Discussion

In the following paragraphs, captopril is abbreviated as Cap. Figure 1 shows the optimized structures, as well as the directions of the dipole moment vectors of the species presently considered. Notice the different orientation/conformation of COOH group in $Cap+Mg^{+2}$ and $Cap+Ca^{+2}$ composites and the decomposed structure of Cap^{+2}.

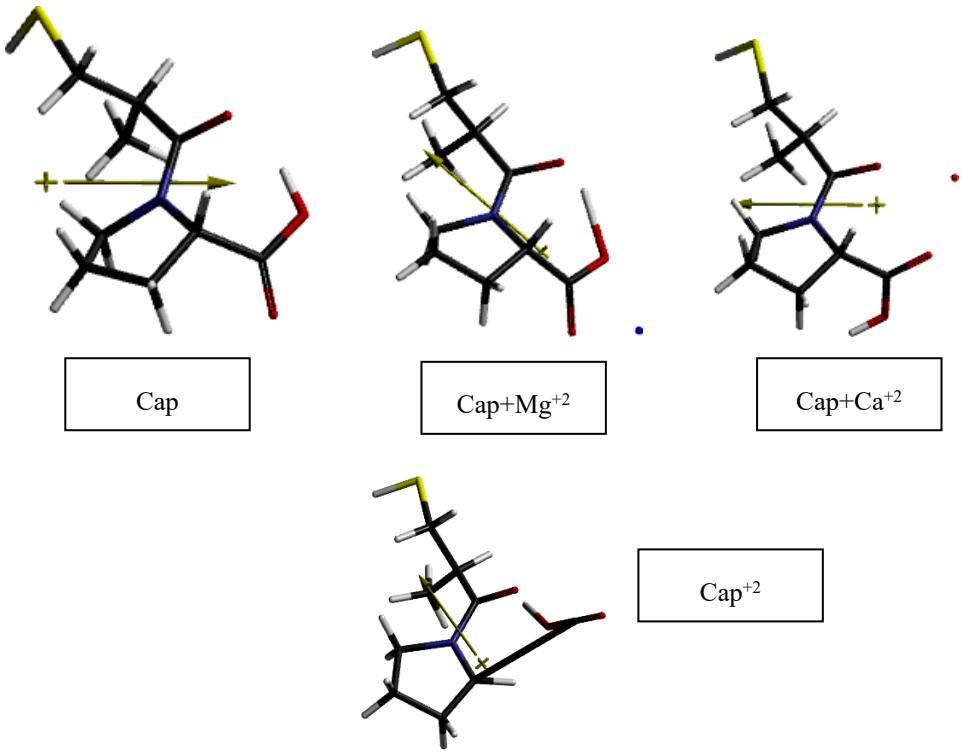

Figure 1. Optimized structures of the species considered.

Table 1 list some thermo chemical properties of the composites considered. Data in the table reveal that the standard heat of formation (H^o) values of the composites are exothermic and they are favored according to their G^o (Gibbs free energy of formation) values.

Table 1. Some thermo chemical properties of the species considered.

Species	H°	S° (J/mol°)	G°
Cap	-2705852.837	457.51	-2705989.233
Cap^{+2}	-2704080.108	476.07	-2704222.044
$Cap+Mg^{+2}$	-3229718.362	479.72	-3229861.375
$Cap+Ca^{+2}$	-4483680.629	485.20	-4483825.269

Energies in kJ/mol.

Table 2 shows some energies of the species considered. Note that E, ZPE and E_C stand for the total electronic energy, zero point vibrational energy and the corrected total electronic energy, respectively [21]. The data in Table 2 reveal that they are all electronically stable structures.

Table 2. Some energies of the species considered.

Species	E	ZPE	E_C
Cap	-2706491.04	627.94	-2705863.1
Cap^{+2}	-2704709.38	617.01	-2704092.37
$Cap+Mg^{+2}$	-3230359.07	632.36	-3229726.71
$Cap+Ca^{+2}$	-4484309.52	631.49	-4483678.03

Energies in kJ/mol.

Figure 2 shows the electrostatic potential (ESP) charges on atoms of Cap, Cap^{+2} and Mg^{+2} and Ca^{+2} composites. Electrostatic charges chosen to best match the electrostatic potential points surrounding a molecule subject to over all charge balance [22,23]. The ESP charges are obtained by the program which uses a numerical method that generates charges, thus reproducing the electrostatic potential field from the entire wavefunction [21].

As seen in the figure in all the cases, the charge of cation components is no longer +2 but a partial charge less than 2 on the metal cations indicates that some electron population has been transferred from the organic component, Cap. Thus, the organic component gets some over all positive charge (see Figure 2).

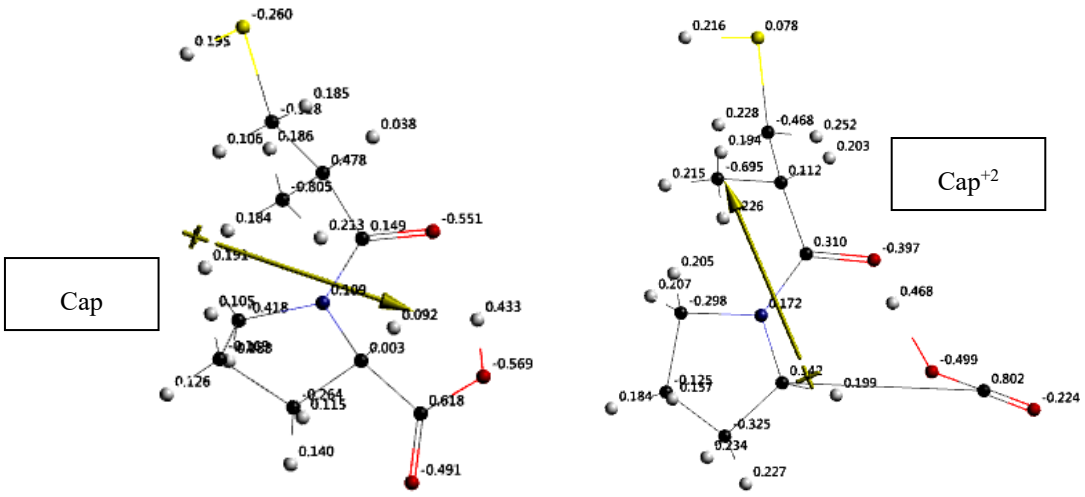

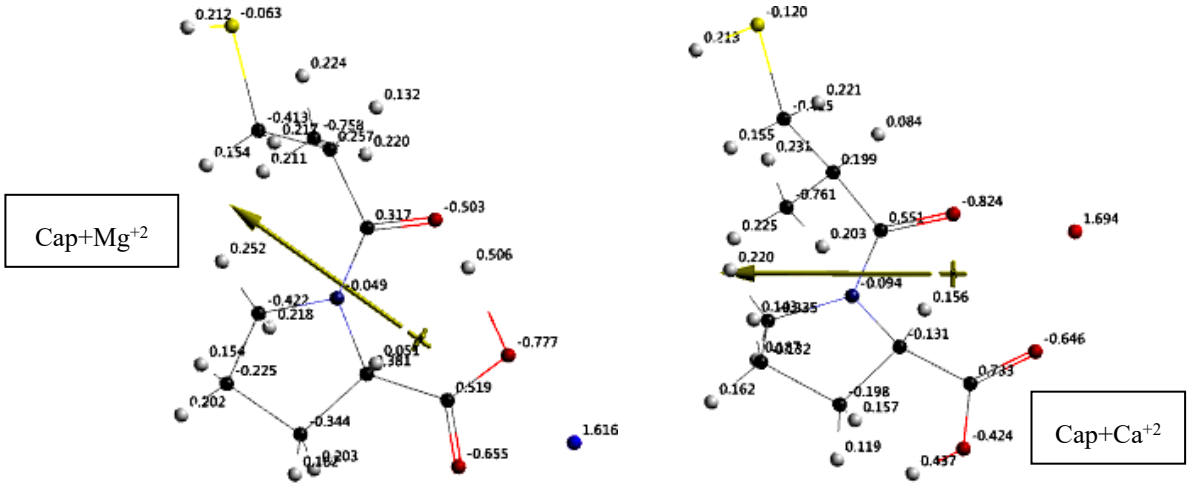

Figure 2. Partial charges on atoms of the species considered.

Figure 3 stands for the exposed area values of atoms of the species considered [21].

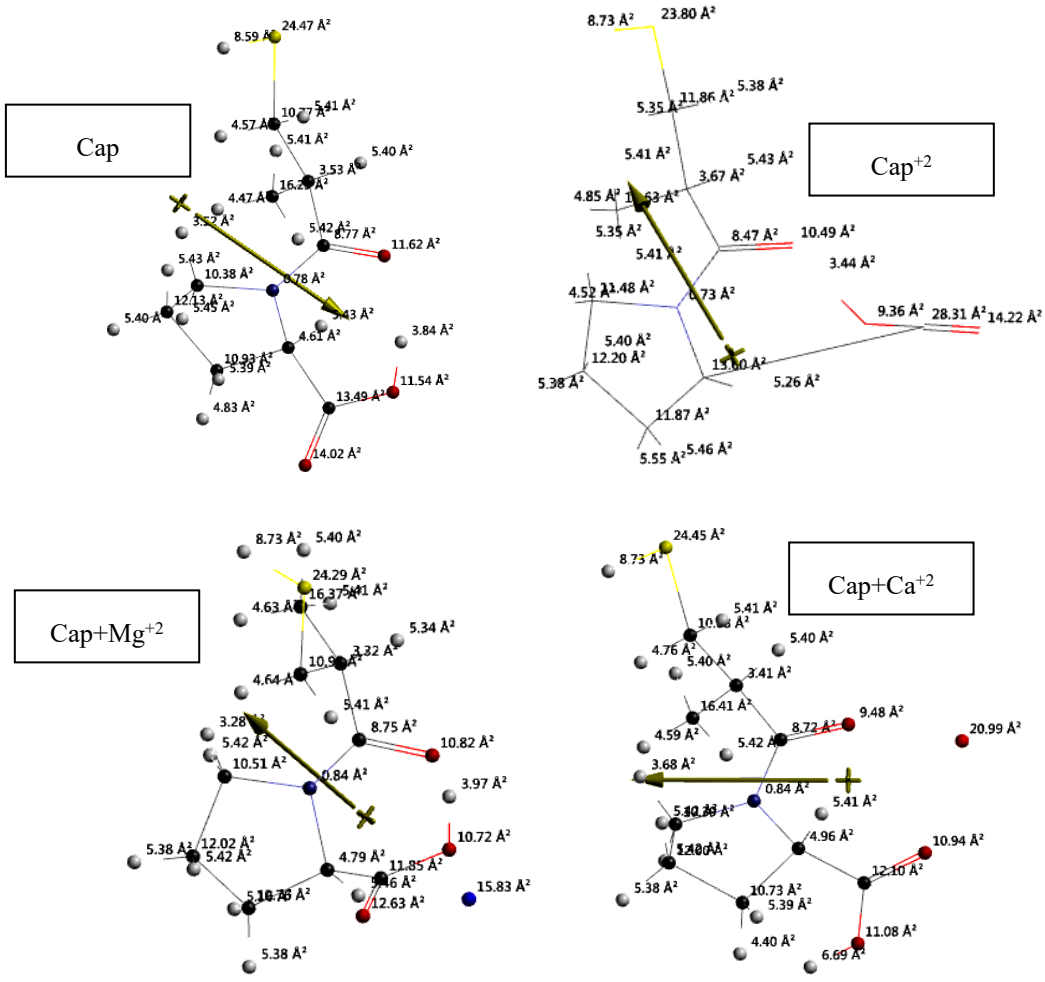

Figure 3. The exposed area values of atoms of some of the species considered.

Figure 4 displays the calculated IR spectrums of the species considered. IR spectrum of Cap has acid COO-H stretch at 3293 cm^{-1}, followed by various C-H stretchings occurring in the region of 3155-3046 cm^{-1}. The acid C=O stretching happens at 1818 cm^{-1} whereas C=O stretching takes place at 1634 cm^{-1}. Another moderately strong peak happens at 1460 and assigned as acid CO-OH bending.

Cap^{+2} is the decomposed structure. Its IR spectrum possesses O-H stretching of the expelled moiety at 3205 cm^{-1} (very strong). Then, a moderately strong peak comes at 2438 cm^{-1} which belongs to the expelled moiety again.

In the IR spectrum of $Cap+Mg^{+2}$ composite various very weak peaks occurring between 3438 cm^{-1} (COO-H stretching) and 3000 cm^{-1} (various C-H stretchings) are observed. The S-H stretch happens at 2700 cm^{-1}, it is a weak vibration. The carbonyl-ring bond stretches at 1605 cm^{-1} coupled with ring breathing vibrations and the COO-H stretch/bending motions.

In the IR spectrum of $Cap+Ca^{+2}$ composite, the O-H stretch happens at 3727 cm^{-1} and then followed by very weak peaks occurring between 3182 and 3000 cm^{-1}. The S-H stretch is also very weak and occurred at 2705 cm^{-1}. A strong peak at 1695 cm^{-1} is COOH stretching coupled with adjacent ring breathing vibrations.

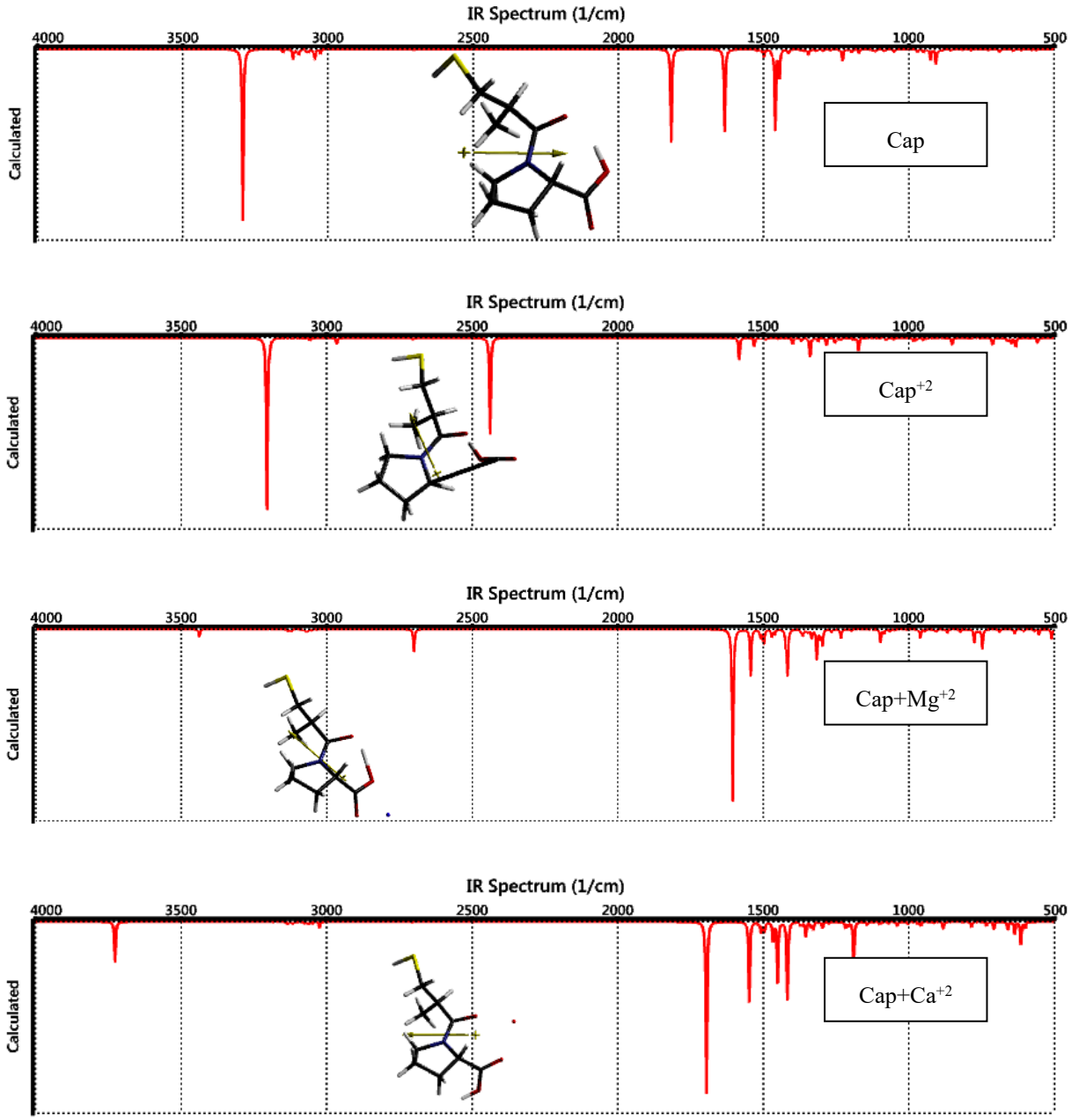

Figure 4. IR spectrums of the species considered.

Electrostatic potential map of the species considered are shown in Figure 5. Note that electro static potential is the energy of interaction of a positive charge with the nuclei and fixed electron distribution of a molecule [22]. In an electrostatic potential map negative potential regions reside on red/reddish and positive ones on blue/bluish parts of the maps. As seen in the figure, the positive charge, in each case affects the whole molecule, thus the local effects are veiled.

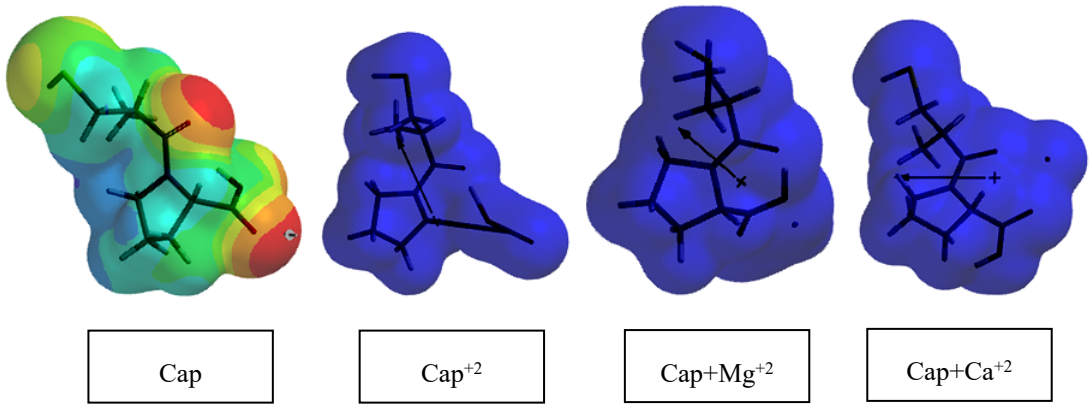

Figure 5. Electrostatic potential maps of the species considered.

Local ionization potential is a measure of the relative ease of electron removal 8ionization)as a function of localization [22]. Figure 6 shows the local ionization potential maps of the species where conventionally red/reddish regions (if any exists) on the density surface indicate areas from which electron removal is relatively easy, meaning that they are subject to electrophilic attack. Note that the local ionization potential map is a graph of the value of the local ionization potential on an isodensity surface corresponding to a van der Waals surface [21,22].

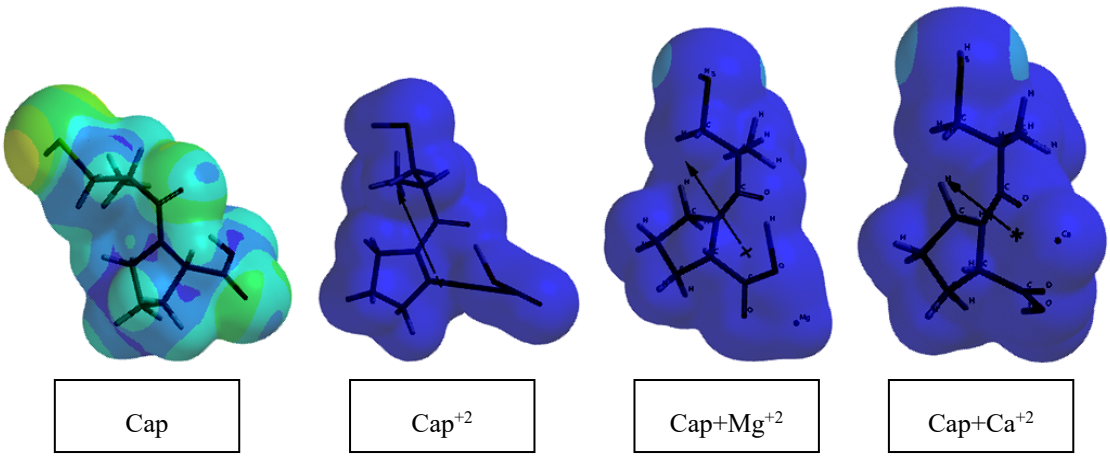

Figure 6. Local ionization potential maps of the species considered.

As seen in the figure the structure, Cap^{+2} is a decomposed molecule and the effect of the positive charge influences both the eliminated moiety and the remnant of the organic part. In the case of the composite structures, $Cap+Mg^{+2}$ and $Cap+Ca^{+2}$, the local ionization potential map has some region nearby the sulfur atom which has some apatite for eletrophiles. It might be due to the effect of d-atomic orbitals of the sulfur atom.

Figure 7 stands for the LUMO maps of the species.

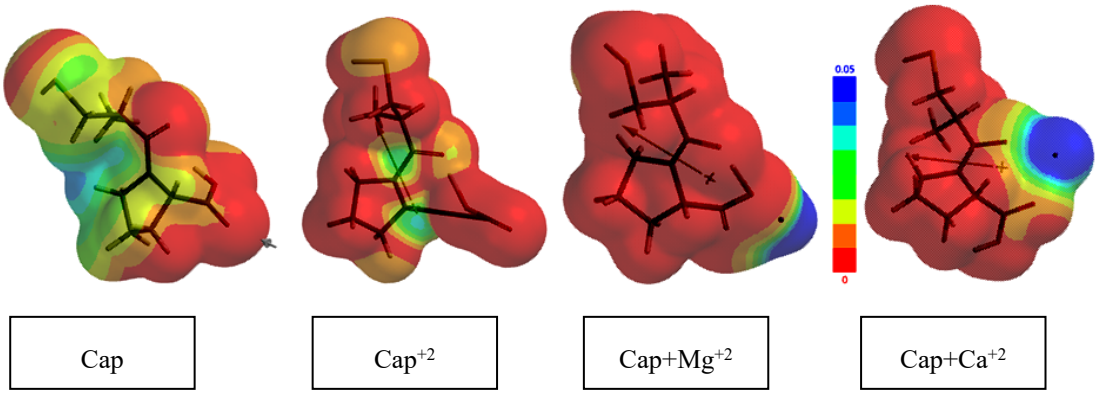

Figure 7. The LUMO maps of the species considered.

Figure 8 stands for the bond densities of Cap, Cap^{+2} and Cap composites considered. Figure clearly indicates that in each case there is no complex formation between the cations considered and the organic component.

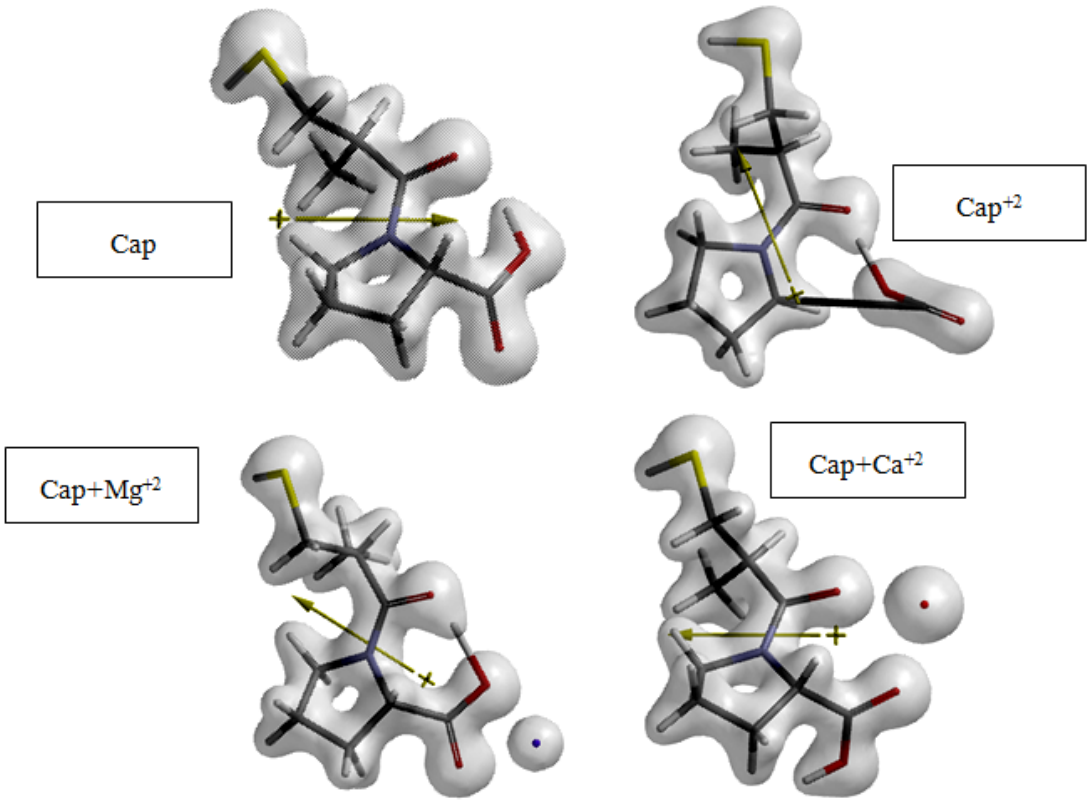

Figure 8. Bond densities of the species considered.

Since bond density surfaces identify regions corresponding to bonding electron density, their size may be roughly correlate with the number of electrons that participate in bonding. Note the bond density between the carbonyl OH hydrogen and the carbonyl oxygen in composite $Cap+Mg^{+2}$ case. There is no hydrogen bonding but probably that hydrogen is in the region of bond density of C=O group.

Figure 9 shows the UV-VIS spectrums (time dependent density functional TDDFT) of the species considered. As seen in the figure the spectrum of dication of Cap spreads over the whole UV-VIS region in contrast to Cap spectrum which covers rather narrow part of the UV region. The spectrums of the composites spread over the large part of the UV-VIS region as well, and mean time new peaks emerge (Table 3).

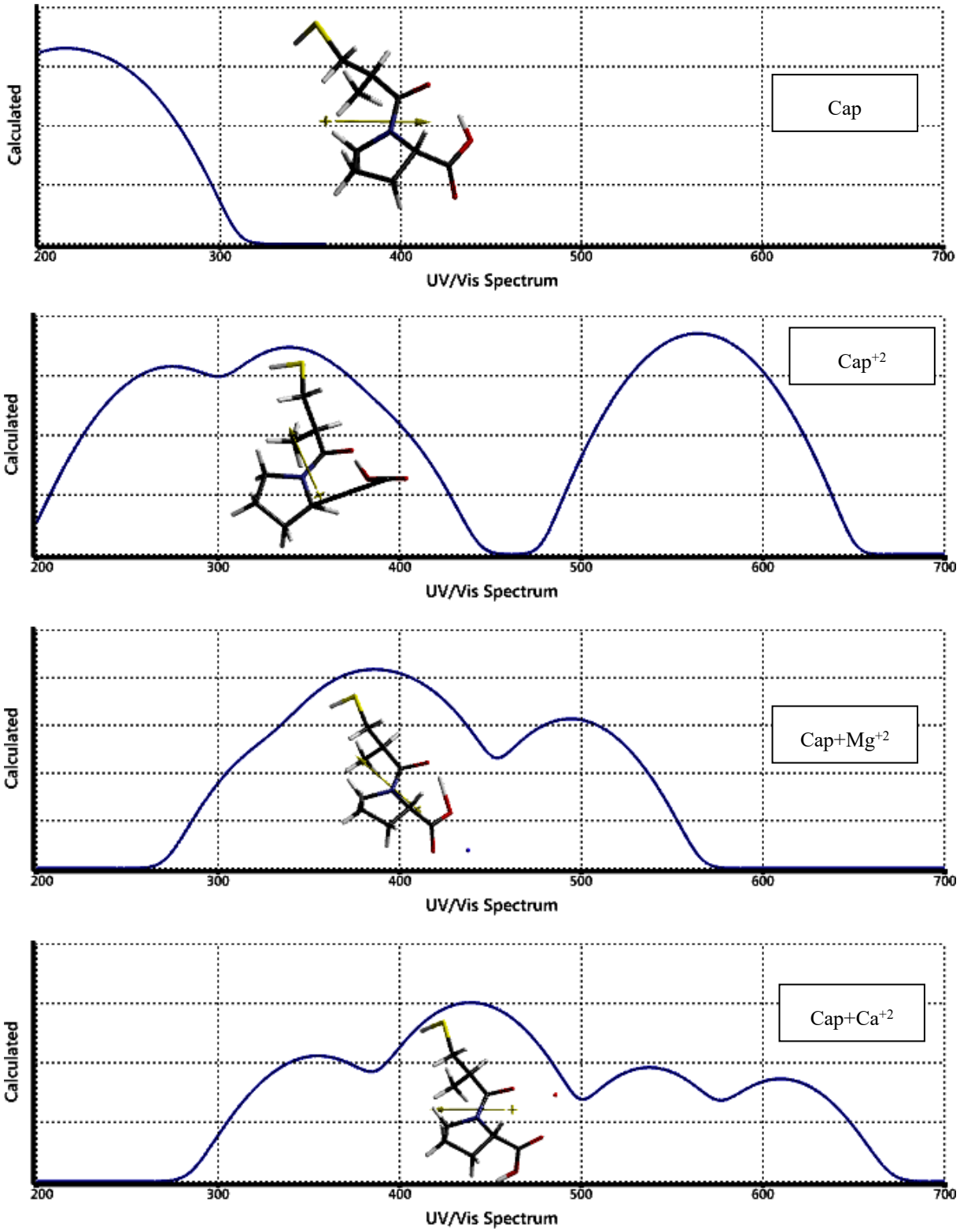

Figure 9. UV-VIS spectrums (TDDFT) of the species considered.

Table 3 lists the λ_{max} values and intensities of the species considered. The spectrum of dication of Cap spreads over the whole UV-VIS region.

Table 3. The λ_{max} values and intensities.

Species	λ_{max} (nm)
Cap	230.45 (0.028)
Cap^{+2}	270.64 (0.015), 277.78 (0.031) 339.05 (0.163), 564.31 (0.366)
$Cap+Mg^{+2}$	378.79 (0.07), 398.51(0.048) 494.41(0.001)
$Cap+Ca^{+2}$	355.39(0.001), 438.95(0.033), 537.39(0.0007), 609.65(0.0003)

Figure 10 is some molecular orbital energy levels of the species considered. Among the charged species (Cap+2 and the composites), $Cap+Mg^{+2}$ has the lowest HOMO-LUMO separation whilst the $Cap+Ca^{+2}$ possesses the largest. Apparently, the charge raises up the HOMO but lowers the LUMO energy levels compared to Cap^{+2} (and Cap).

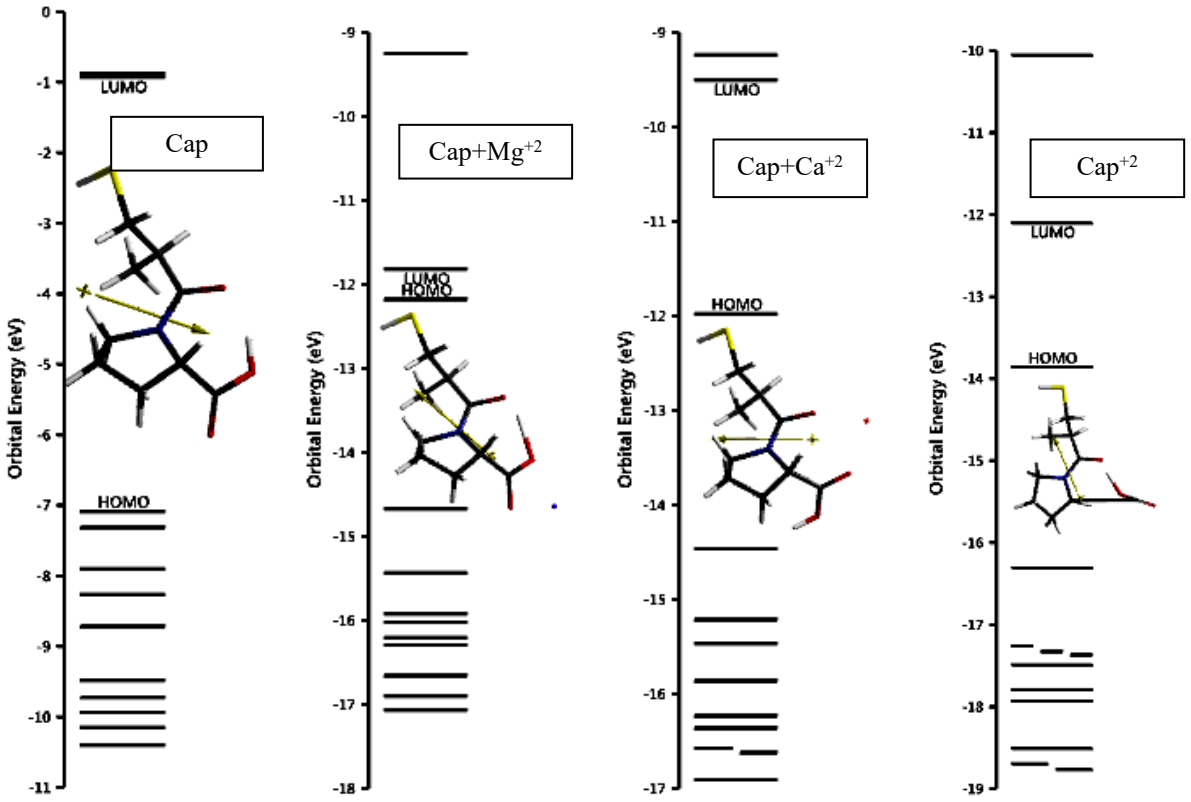

Figure 10. Some of the molecular orbital energy levels of the species considered.

Table 4 lists the HOMO, LUMO energies and Δε values (in kJ/mol.) of the species considered.

Table 4. The HOMO, LUMO energies and Δε values of the species considered.

Species	HOMO	LUMO	Δε
Cap	-683.86	-89.37	594.49
Cap^{+2}	-1337.15	-1167.57	169.58
$Cap+Mg^{+2}$	-1175.16	-1140.26	34.9
$Cap+Ca^{+2}$	-1155.48	-917.09	238.39

Energies in kJ/mol.

The HOMO and LUMO patterns of the species considered are shown in Figure 11. As seen all the species possess π-symmetry. In the composites, the inorganic component does not contribute to the HOMO but the largest contribution to the LUMO is supplied by the inorganic component.

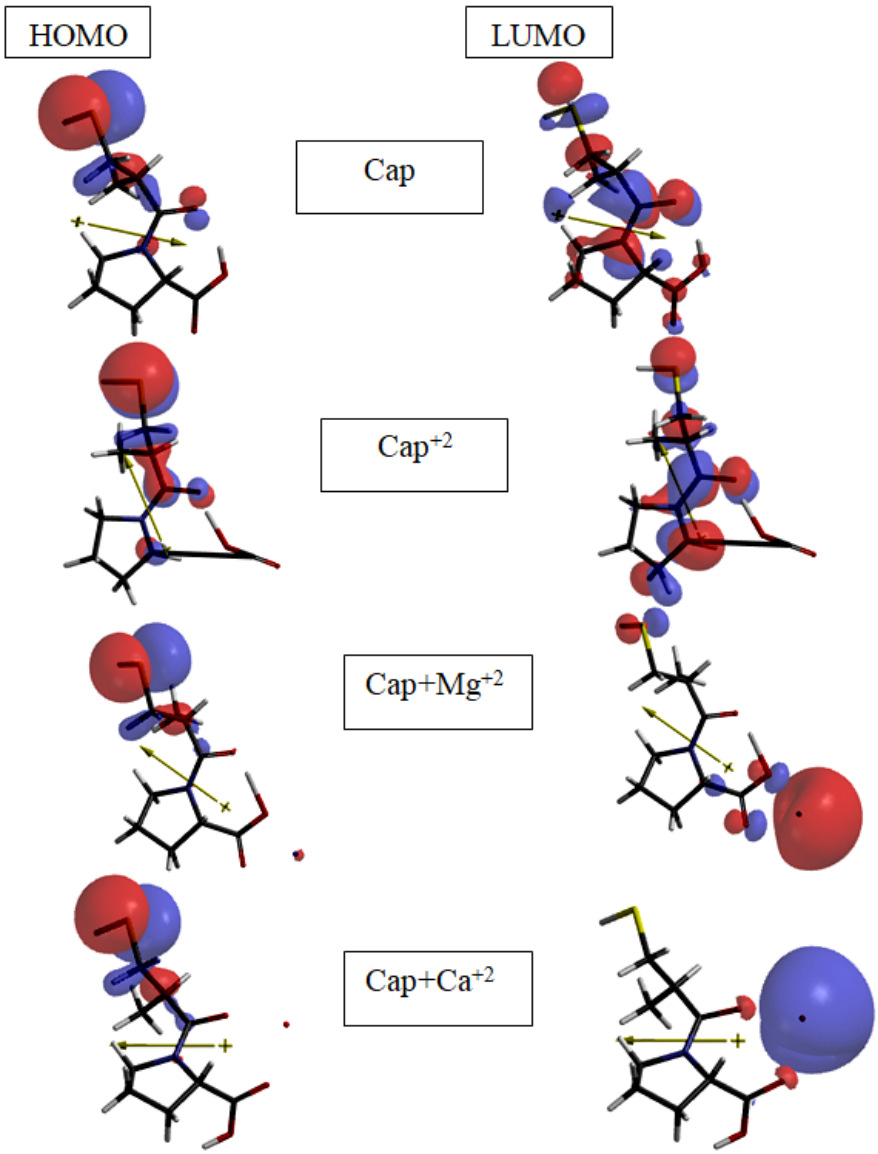

Figure 11. The HOMO and LUMO patterns of the species considered.

Some and properties of the species considered are shown in Tables 5 (geometrical) and 6, respectively.

Table 5. Some geometrical properties of the species considered.

Species	Area (Å²)	Volume (Å³)	Ovality	PSA (Å²)
Cap	231.84	210.27	1.36	41.796
Cap^{+2}	256.62	221.07	1.45	38.246
$Cap+Mg^{+2}$	243.51	218.38	1.39	38.994
$Cap+Ca^{+2}$	248.81	223.20	1.40	39.024

Table 6. Some other properties of the species considered.

Species	Dipole (debye)	Polarizability	Log P	Eaq (kJ/mol)	Cv (J/molº)
Cap	6.08	56.97	0.24	-2706549.44	167.50
Cap^{+2}	3.08	58.89	0.24	-2705709.13	174.71
$Cap+Mg^{+2}$	23.34	59.01	-	-	180.84
$Cap+Ca^{+2}$	19.06	58.90	-	-	182.27

Polarizabilities in 10^{-30} m^3 units

The presence of the dications highly dictates the value of the dipole moment of the composite systems. The effect of magnesium dication is more pronounced over the dication of calcium. Note that the net dipole moment is the vectorial sum of bond dipoles on which local charges, bond lengths, thus some geometrical factors are influential.

The polarizability is defined according to the formula [21].

$$\text{Polarizability} = 0.08*V - 13.0353*h + 0.979920* h^2 + 41.3791$$

where V and h are the Van der Waals volume and hardness, respectively. Hardness is defined as,

$$\text{Hardness} = -(\varepsilon_{HOMO} - \varepsilon_{LUMO})/2$$

where ε_{HOMO} and ε_{LUMO} stand for the energies of the interfrontier molecular orbitals, the HOMO and LUMO, respectively.

On the other hand, one has to consider that in vivo conditions both the Cap and the cations presently considered might be not in the bare form but probably hydrated or complexed.

4. Conclusion

The present DFT treatment, within the restrictions of the density functional theory, at the level of B3LYP/6-311++G(d,p) reveals that in vacuum conditions the Mg^{+2} and Ca^{+2} composites of Captopril have exothermic heat of formation values and favorable Gibbs free energy of formation values. All the composites considered are electronically stable. The collected data reveal that some electron population is transferred from organic component of the composite to the cation so it possesses some partial charge less than the initial formal charge of two. The bond density calculations of the species considered indicates that no bonding interaction exists

between the organic and inorganic components of the composites. However, charge-dipole interactions and interactions through-space might be operating.

The smallest HOMO-LUMO separation in the composite Cap+Mg^{+2} whilst the largest in Cap+Ca^{+2} is intriguing property arising from the relative sizes of the cations and consequent optimized structures.

The present results beside its own merits might be the starting platform for more elaborate studies, especially for some activity-structure calculations.

On the other hand, captopril should be considered an exciting member of the therapeutic armamentarium. It, and pharmacologically related compounds of the future, probably will continue to generate much interest as their final place in therapy becomes better defined through additional well designed studies and wider clinical tests.

References

[1] Heel, R. C., Brogden, R. N., Speight, T. M., & Avery, G. S. (1980). Captopril: A preliminary review of its pharmacological properties and therapeutic efficacy. *Drugs, 20*(6), 409–452. https://doi.org/10.2165/00003495-198020060-00001

[2] Benowitz, N. L., & Bourne, H. R. (1984). Antihypertensive agents. In B. G. Katzung (Ed.), *Basic and clinical pharmacology* (2nd ed., pp. 134–153). Lange Medical Publications.

[3] Frohlich, E. D., Cooper, R. A., & Lewis, E. J. (1984). Review of the overall experience of captopril in hypertension. *Archives of Internal Medicine, 144*(7), 1441–1444. https://doi.org/10.1001/archinte.1984.00350190137023

[4] Fouad, A. A., Al-Mulhim, A. S., Jresat, I., & Morsy, M. A. (2013). Protective effects of captopril in diabetic rats exposed to ischemia/reperfusion renal injury. *Journal of Pharmacy and Pharmacology, 65*(2), 243–252. https://doi.org/10.1111/j.2042-7158.2012.01585.x

[5] Nagasawa, T. H., Khan, M. A., & Imig, J. D. (2012). Captopril attenuates hypertension and renal injury induced by the vascular endothelial growth factor inhibitor sorafenib. *Clinical and Experimental Pharmacology and Physiology, 39*(5), 454–461. https://doi.org/10.1111/j.1440-1681.2012.05699.x

[6] Dondi, M., Franchi, R., Levorato, M., Zuccala, A., Gaggi, R., Mirelli, M., Stella, A., Marchetta, F., Losinno, F., & Monetti, N. (1989). Evaluation of hypertensive patients by means of captopril enhanced renal scintigraphy with technetium-99m DTPA. *Journal of Nuclear Medicine, 30*(5), 615–621.

[7] Geyskes, G. G., Oei, H. Y., Puylaert, C. B., & Mees, E. J. (1987). Renovascular hypertension identified by captopril-induced changes in the renogram. *Hypertension, 9*(5), 451–458. https://doi.org/10.1161/01.hyp.9.5.451

[8] Mann, S. J., Pickering, T. G., Sos, T. A., Uzzo, R. G., Sarkar, S., Friend, K., Rackson, M. E., & Laragh, J. H. (1991). Captopril renography in the diagnosis of renal artery stenosis: Accuracy and limitations. *American Journal of Medicine, 90*(1), 30–40. https://doi.org/10.1016/0002-9343(91)90503-P

[9] Oei, H. Y., Geyskes, G. G., Mees, E. J., & Puylaert, C. B. (1987). The significance of captopril renography in renovascular hypertension. *Contributions to Nephrology, 56*, 95–103. https://doi.org/10.1159/000413788

[10] Setaro, J. F., Saddler, M. C., Chen, C. C., Hoffer, P. B., Roer, D. A., Markowitz, D. M., Meier, G. H., Gusberg, R. J., & Black, H. R. (1991). Simplified captopril renography in diagnosis and treatment of renal artery stenosis. *Hypertension, 18*(3), 289–298. https://doi.org/10.1161/01.hyp.18.3.289

[11] Sfakianakis, G. N., Bourgoignie, J. J., & Jaffe, D. (1987). Single-dose captopril scintigraphy in the diagnosis of renovascular hypertension. *Journal of Nuclear Medicine, 28*(9), 1383–1392.

[12] Bolterman, R. J., Manriquez, M. C., Ruiz, M. C. O., Juncos, L. A., & Romero, J. C. (2005). Effects of captopril on the renin angiotensin system, oxidative stress, and endothelin in normal and hypertensive rats. *Hypertension, 46*(4), 943–947. https://doi.org/10.1161/01.HYP.0000174602.59935.d5

[13] Stewart, J. J. P. (1989). Optimization of parameters for semi-empirical methods I. *Journal of Computational Chemistry, 10*(2), 209–220. https://doi.org/10.1002/jcc.540100208

[14] Stewart, J. J. P. (1989). Optimization of parameters for semi-empirical methods II. *Journal of Computational Chemistry, 10*(2), 221–264. https://doi.org/10.1002/jcc.540100209

[15] Leach, A. R. (1997). *Molecular modeling*. Longman.

[16] Kohn, W., & Sham, L. J. (1965). Self-consistent equations including exchange and correlation effects. *Physical Review, 140*(4A), 1133–1138. https://doi.org/10.1103/PhysRev.140.A1133

[17] Parr, R. G., & Yang, W. (1989). *Density functional theory of atoms and molecules*. Oxford University Press.

[18] Becke, A. D. (1988). Density-functional exchange-energy approximation with correct asymptotic behavior. *Physical Review A, 38*(6), 3098–3100. https://doi.org/10.1103/PhysRevA.38.3098

[19] Vosko, S. H., Wilk, L., & Nusair, M. (1980). Accurate spin-dependent electron liquid correlation energies for local spin density calculations: A critical analysis. *Canadian Journal of Physics, 58*(8), 1200–1211. https://doi.org/10.1139/p80-159

[20] Lee, C., Yang, W., & Parr, R. G. (1988). Development of the Colle-Salvetti correlation energy formula into a functional of the electron density. *Physical Review B, 37*(2), 785–789. https://doi.org/10.1103/PhysRevB.37.785

[21] Wavefunction Inc. (2006). SPARTAN 06 (Version 1.0). Wavefunction Inc.

[22] Wavefunction Inc. (2006). TRIDENT: Molecular modeling for medicinal chemists. Wavefunction Inc.

[23] Wavefunction Inc. (2006). SPARTAN: Molecular modeling in physical chemistry. Wavefunction Inc.